Modulation of population inversion in N_2^+ by a pump-control-seed scheme

Siqi Wang,[1,*] Erik Lötstedt,[2,*] Jincheng Cao,[1] Yao Fu,[1] Hongwei Zang,[1] Helong Li,[1,3] Kaoru Yamanouchi,[2,†] and Huailiang Xu[1,4,5,‡]

[1]*State Key Laboratory of Integrated Optoelectronics, College of Electronic Science and Engineering, Jilin University, Changchun 130012, China*

[2]*Department of Chemistry, School of Science, The University of Tokyo, 7-3-1 Hongo, Bunkyo-ku, Tokyo 113-0033, Japan*

[3]*Institute of Atomic and Molecular Physics, Jilin University, Changchun 130012, China*

[4]*State Key Laboratory of Precision Spectroscopy & Chongqing Institute, East China Normal University, Shanghai 200062, China*

[5]*CAS Center for Excellence in Ultra-Intense Laser Science, Shanghai 201800, China*

(Received 5 June 2022; accepted 7 September 2022; published 19 September 2022)

We experimentally demonstrate an externally seeded N_2^+ lasing action on the transition between the $B\,^2\Sigma_u^+(v=0)$ and $X\,^2\Sigma_g^+(v'=0)$ states at 391.4 nm by irradiating a N_2 gas with an intense 400-nm pump laser pulse and reveal that the populations in the rotational levels of $J'=7$–17 in the $B\,^2\Sigma_u^+(v=0)$ state are responsible for the lasing based on the rotational revival structure in the lasing intensity recorded by the pump-probe measurements. By introducing additionally an 800-nm control pulse, we find that the lasing intensity is suppressed when the timing of the control pulse is set between the 400-nm pump and 400-nm seed laser pulses while it can be enhanced when the control pulse overlaps temporally the seed pulse. By solving the time-dependent Schrödinger equation including the continuous ionization of N_2 and multistate coupling among the $B\,^2\Sigma_u^+$, $A\,^2\Pi_u$, and $X\,^2\Sigma_g^+$ states in N_2^+ induced by the control pulse, we show that the population inversion in N_2^+ can be achieved by the 400-nm pump laser pulse and can be further modulated by the control pulse. We show also that the N_2^+ lasing intensity can be suppressed or enhanced depending on the timing and intensity of the control pulse originating from the competition between the two dynamical processes, that is, the ionization of N_2 and the population transfer among the three electronic states of N_2^+.

DOI: 10.1103/PhysRevA.106.033110

I. INTRODUCTION

The propagation of intense femtosecond (fs) laser pulses in atomic and molecular gases can induce characteristic strong-field phenomena, such as the generation of high-order harmonics [1], molecular orientation and alignment [2], ionization and excitation of molecules [3,4], chemical reactions for laser ignition [5,6], and air lasing [7–9]. Among these findings, air lasing generated with atmospheric constituents as gain media has attracted much attention in recent years thanks to its promising applications in remote detection of atmospheric pollutants and greenhouse gases [10–17]. In particular, the N_2^+ air lasing has widely been studied so far because of its intriguing and complex generation mechanisms. It was observed in earlier experiments that the lasing emission of N_2^+ can be generated by the irradiation of N_2 with 800-nm strong-laser pulses [18]. However, according to the Ammosov-Delone-Krainov ionization model [19], the optical amplification on this transition cannot be interpreted only by the ionization of N_2 by the 800-nm laser field. Therefore, a number of different physical models have been proposed to explain this lasing phenomenon, such as postionization recollision [20] and multistate coupling [21–25] producing the population inversion and lasing without population inversion [26–28].

Interestingly, it was demonstrated that the generation mechanism of this lasing emission is dependent on the wavelength of the pump laser [29–31]. So far, both theoretical and experimental results obtained at the pump laser wavelength of around 800 nm have revealed that, after the ionization of N_2, the rear part of the laser pulse will induce a population transfer from the $X^2\,\Sigma_g^+$ state to the $A\,^2\Pi_u$ states through a one-photon resonance coupling process, leading to a population redistribution in N_2^+, so that the lasing action occurs [23]. In the case of the pumping by midinfrared wavelength laser, near-resonant stimulated Raman scattering provides a possibility of producing the lasing emission [29]. Recently, we experimentally showed that intense near-UV femtosecond laser pulses at around 400 nm can induce the lasing actions of N_2^+ at 423.6 and 427.8 nm, corresponding, respectively, to the $B\,^2\Sigma_u^+ - X\,^2\Sigma_g^+$ (1, 2) and (0, 1) transitions, whose mechanism has been explained theoretically in terms of the population inversion induced by a Rabi oscillation combined with a Raman-type transition [30]. For the lasing emission at 391.4 nm on the $B\,^2\Sigma_u^+ - X\,^2\Sigma_g^+$ (0, 0) transition achieved by the 400-nm laser excitation, its generation mechanism has not yet been explored well [31].

In the present study, we systematically investigate the N_2^+ lasing at 391.4 nm using a pump-control-seed scheme, in

*These authors contributed equally to this work.
†kaoru@chem.s.u-tokyo.ac.jp
‡huailiang@jlu.edu.cn

which a chirped 400-nm laser (pump) is employed to ionize N_2 and induce the population inversion in N_2^+, which is subsequently seeded in a picosecond delay time by a weak 400-nm light (seed). An 800-nm laser (control) is then used to manipulate the N_2^+ lasing action. With this scheme, we observe the molecular alignment-dependent oscillations of the lasing intensity and find that the populations responsible for the lasing are mainly lying on the rotational levels of $J' = 7$–17 in the electronically excited $B\,^2\Sigma_u^+$ ($v = 0$) state of N_2^+. We also demonstrate that the lasing emission can be manipulated well by the control pulse, which can induce significant suppression contrary to the enhancement achieved by pumping at 800 nm [32,33]. By numerical simulations of the population distribution in the $X\,^2\Sigma_g^+$, $B\,^2\Sigma_u^+$, and $A\,^2\Pi_u$ states of N_2^+, we demonstrate that the population inversion between the $B\,^2\Sigma_u^+$ and $X\,^2\Sigma_g^+$ states of N_2^+ can be achieved by the intense 400-nm laser pumping pulse and can be efficiently modulated by the control pulse through the competition between the ionization of N_2 and the postionization coupling among the three electronic states of N_2^+. We also reveal that both the ionization and postionization coupling are influenced sensitively by the light-field parameters, which is in accordance with the experimental observations.

II. EXPERIMENTAL SETUP

The laser source used in the experiment was launched from a Ti:sapphire amplification system (Spectra Physics, Spitfire ACE), which produces linearly polarized 800-nm femtosecond laser pulses with a repetition rate of 200 Hz, a single pulse energy of ~8 mJ, and a chirped pulse duration of ~400 fs. The output 800-nm laser beam was split into three beams by two beam splitters. The first 800-nm laser beam was frequency doubled in a β-barium borate (BBO) crystal (thickness 200 μm, diameter 10 mm) to produce an intense 400-nm pump with the pulse energy of ~400–500 μJ. The second 800-nm laser beam with the central wavelength of 800 nm was used as a control laser beam whose energy was modulated by a half wave plate and a polarizer, and the third 800-nm laser beam was frequency doubled in another BBO crystal (thickness 300 μm, diameter 5 mm) to produce a weak 400-nm seed with the pulse energy of 0.6–0.9 μJ. The contamination of the 800-nm fundamental light in the 400-nm pump and seed laser beams is completely eliminated by five dichroic mirrors with high reflectivity (99.5%) at 400 nm and high transmission (95%) at 800 nm. One additional dichroic mirror was used to combine the pump–seed laser beam with the control laser beam. An 800-nm half wave plate and a 400-nm half wave plate were inserted, respectively, in the control and seed beams to modulate their polarization directions, so that the polarization directions of the pump, seed, and control laser pulses can be arranged to be parallel or perpendicular to each other.

A motorized delay stage with a temporal resolution of about 10 fs was placed in each of the pump beam path and the control beam path to regulate the delay time of the pump and control laser pulses with respect to the seed pulse. The pump laser beam was focused by a fused silica lens ($f = 30$ cm) into a nitrogen gas chamber (20 mbar), and the seed laser beam was focused by another fused silica lens ($f = 30$ cm) and crossed with the pump laser beam at a crossing angle of about 4°. After being focused by an $f = 40-$cm fused silica lens, the control laser beam propagates in a collinear scheme either with the seed beam or the pump beam into the chamber. Hereafter, we refer to these two schemes as the "collinear control-seed" scheme [Fig. 1(a)] and the "collinear pump-control" scheme [Fig. 1(b)]. In the experiments, these two schemes were switched by replacing the two beam splitters by those having different splitting energy ratios and exchanging the BBO crystals in the pump and seed beam paths. The intensity of the pump beam at the focus under the vacuum conditions was calculated to be ~5–6 $\times 10^{14}$ W/cm^2, if the plasma defocusing effect is neglected.

After passing through the gas chamber, the forward lasing produced through the externally seeded scheme [Fig. 1(c)] in the seed beam direction was collimated by a fused silica lens ($f = 30$ cm), and then, passed through two mirrors with high reflectivity at around 400 nm. Two additional mirrors with high reflectivity at 800 nm and high transmission at 400 nm were inserted in the light beam path to reflect the 800-nm control laser pulses. The N_2^+ lasing at 391.4 nm was then focused by a focal lens ($f = 6$ cm) and finally detected by a spectrometer (Andor Shamrock SR-303i) equipped with a 1200-grooves per millimeter grating and coupled with an intensified charge coupled device (ICCD) camera (Andor iStar). The gate delay and gate width of the ICCD camera were set to be at −5 and 50 ns, respectively. All the spectral data in the experiments were accumulated over 1000 laser shots.

III. EXPERIMENTAL RESULTS

Figure 1(d) shows the forward spectrum (red solid) collected along the seed beam in the collinear pump-control scheme with no control pulse. For comparison, the spectra measured with the seed-only (blue dashed line) and pump-only (black dashed-dotted line) are also shown. The pump-only spectrum was measured by recording the scattering light from the pump beam with the detector being set on the propagation axis of the seed beam. It can be seen in Fig. 1(d) that a 391.4-nm lasing peak appears on the top of the seed-only spectrum when the pump pulse is present, which is more clearly seen after the subtraction of the seed spectrum as shown in the inset of Fig. 1(d). In the seed amplification scheme, the lasing intensity I_{laser} in Fig. 1(d) can be given by $I_{\text{laser}} = I_{\text{seed}}e^{gL}$, where g and L are the gain coefficient and the length of the gain medium, respectively. Using the waist diameter of the seed laser beam and the crossing angle between the pump and seed laser beams, the length L is estimated to be $L = 440$ μm. Then, from the intensity ratio of $I_{\text{laser}}/I_{\text{seed}} = 1.94$ obtained from the spectra shown in Fig. 1(d), the gain coefficient is estimated to be $g = 15$ cm^{-1}, which is comparable to that obtained previously by the pumping at 800 nm [34]. The sharp peak appearing at 391.4 nm corresponds to the head of the P-branch rotational transitions ($J - 1 \rightarrow J$), and the peak appearing at around 390.2 nm corresponds to the R-branch rotational transitions ($J + 1 \rightarrow J$) of the $B\,^2\Sigma_u^+ - X\,^2\Sigma_g^+(0,\ 0)$ transition.

We recorded the intensity of the P-branch head at 391.4 nm as a function of the time delay between the pump and seed

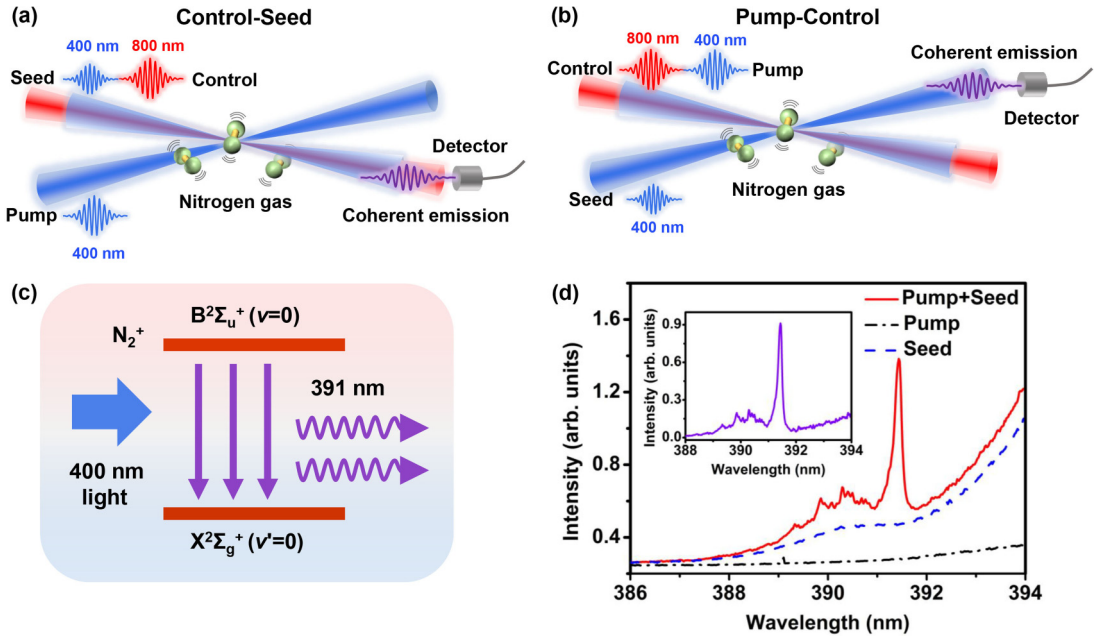

FIG. 1. Schematic diagrams of the experimental setups in (a) the collinear control-seed scheme and (b) the collinear pump-control scheme. (c) Energy-level diagrams of N_2^+ and the corresponding 391.4-nm lasing transitions induced by 400-nm laser pulses. (d) The 391.4-nm lasing spectrum for the forward emission recorded with the pump-control scheme (red solid line) with no control pulse, the seed-only (blue dashed line) scheme, and the pump-only (black dashed-dotted line) scheme. The inset shows the 391.4-nm lasing spectrum with the seed background eliminated.

pulses for the cases when the polarization direction of the pump laser pulse is parallel (red solid line) and perpendicular (blue dotted line) to that of the seed laser pulse as shown in Fig. 2(a), where the baseline is obtained from the subtraction of the lasing signals by the seed level. The zero delay represents the timing when the lasing starts to appear, and the positive delay represents the seed pulse being injected after the pump pulse. It can be seen in Fig. 2(a) that both curves exhibit a sudden increase after the zero delay and a slow exponential decay superposing a characteristic intensity oscillation representing the rotational revivals of N_2^+ [34,35]. This rotational revival structure shows that a coherent rotational wave packet is formed by the nonadiabatic rotational alignment of N_2 induced by the 400-nm pump laser pulse. The synchronous antiphase oscillations obtained under the perpendicular and parallel conditions are ascribed to the difference in the corresponding values of the azimuthal quantum number M in these two cases [35].

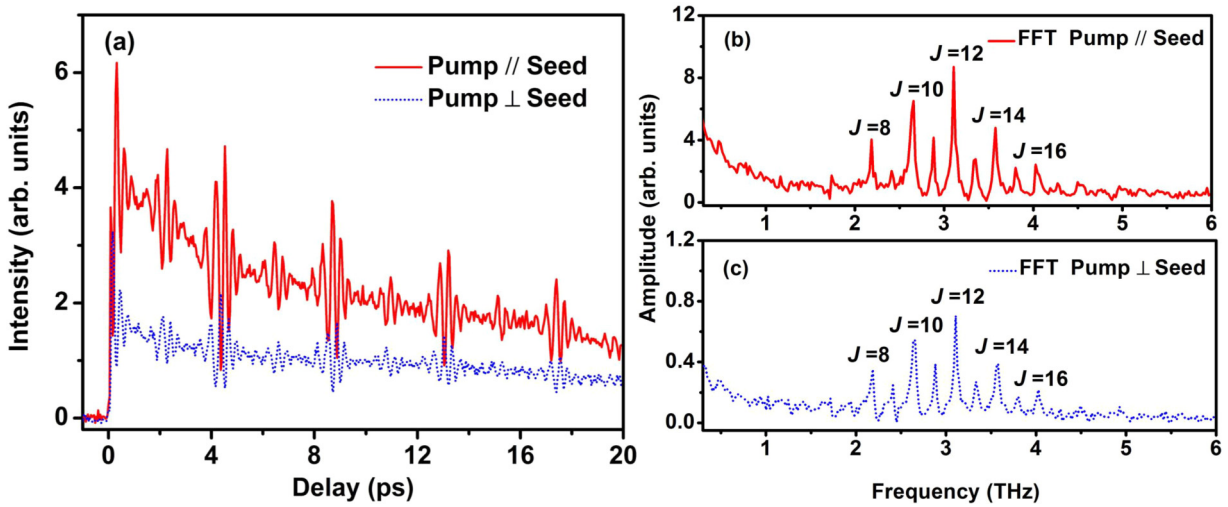

FIG. 2. (a) Intensity of the P-branch head of the $B\,^2\Sigma_u^+ - X\,^2\Sigma_g^+(0,\ 0)$ emission of N_2^+ at around 391.4 nm recorded as a function of the time delay between the pump pulse and the seed pulse for the two cases in which the polarization directions of the pump and seed pulses are parallel (red solid line) and perpendicular (blue dotted line) to each other. (b) The Fourier transform spectrum for the parallel polarization configuration and (c) that for the perpendicular polarization configuration obtained by the Fourier transform of the respective traces in (a).

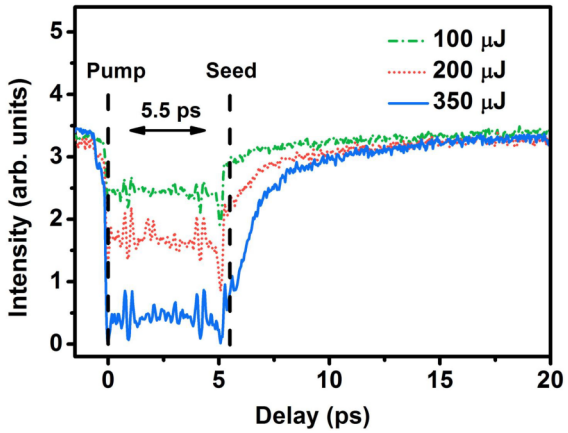

FIG. 3. The 391.4-nm signal intensity obtained by scanning the 800-nm control laser pulse at the different energies in the time range of −1.5–20 ps for the collinear control-seed scheme. The time interval $\Delta t_{\mathrm{pump-seed}}$ between the pump and seed pulses is 5.5 ps. The rotational revival structure appearing in the temporal range of $\Delta t_{\mathrm{pump-control}} = 0$–5.5 ps reflects the field-free molecular alignment induced by the pump pulse.

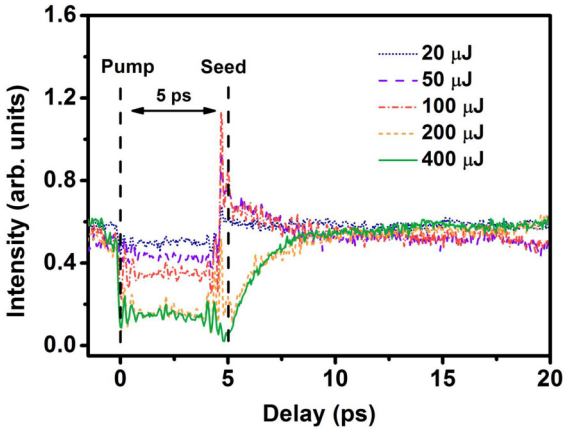

FIG. 4. The 391.4-nm lasing signal intensity obtained by scanning the 800-nm control laser pulse at the five different pulse energies in the collinear pump-control scheme. The temporal separation $\Delta t_{\mathrm{pump-seed}}$ between the pump and seed pulses is set to be 5 ps.

To explore the origin of the rotational revivals, we convert the two traces shown in Fig. 2(a) into the frequency domain by a Fourier transform (FT). The resultant FT spectra are shown in Figs. 2(b) and 2(c), both of which exhibit almost the same spectral structures. Based on the beat frequencies $\Omega = \frac{E_{J+2}-E_J}{h} = (4J+6)Bc$, where B is the rotational constant, c is the speed of light, and J is the rotational quantum number, the respective peaks appearing in the FT spectra can be assigned to the separations among the rotational energy levels of $J = 8$–16 in the $X\ ^2\Sigma_g{}^+$ state of $N_2{}^+$ with the rotational constant of $B_{v=0} = 1.932\ \mathrm{cm}^{-1}$ [36], showing that the emission transitions from the upper rotational levels $J' = 7$–17 contribute to the $B\ ^2\Sigma_u{}^+ - X\ ^2\Sigma_g{}^+$ (0, 0) lasing emission of $N_2{}^+$ at 391.4 nm in the present collinear pump-control scheme. As has been demonstrated in our recent study [37], the $X\ ^2\Sigma_g{}^+$, $A\ ^2\Pi_u$, and $B\ ^2\Sigma_u{}^+$ states of $N_2{}^+$, which are coherently coupled by an 800-nm laser field, exhibit different degrees of the rotational excitation. Indeed, a rotational wave packet is created clearly in the $X\ ^2\Sigma_g{}^+$ state, but the evolution of the rotational wave packet cannot be identified well in the $A\ ^2\Pi_u$ state, which is resonantly coupled by the 800-nm laser field with the $X\ ^2\Sigma_g{}^+$ state. In the present case, in a similar manner as in the case of the $A\ ^2\Pi_u - X\ ^2\Sigma_g{}^+$ resonance excitation at 800 nm, it is possible that the resonance coupling between the $B\ ^2\Sigma_u{}^+$ and $X\ ^2\Sigma_g{}^+$ state at 400 nm efficiently creates a rotational wave packet only in the $X\ ^2\Sigma_g{}^+$ state, resulting in the modulation of the $B\ ^2\Sigma_u{}^+ - X\ ^2\Sigma_g{}^+$ lasing emission reflecting the rotational wave packet propagation in the $X\ ^2\Sigma_g{}^+$ state.

In Fig. 3, we show the variation of the signal intensity of the lasing at 391.4 nm integrated over the spectral range of 391.2–391.5 nm recorded in the presence of the control pulse with the collinear control-seed scheme. In this measurement, the temporal separation between the pump pulse and the seed pulse was fixed at 5.5 ps and the control pulse was scanned in the time range between $\Delta t_{\mathrm{pump-control}} = -1.5$ and 20 ps. The polarization directions of the three pulses are all parallel to each other. This scan was performed at the three different pulse energies (100, 200, and 350 μJ) of the control laser pulse. The zero delay of $\Delta t_{\mathrm{pump-control}} = 0$ ps represents the temporal overlap of the pump and control pulses. It can be seen in Fig. 3 that the 391.4-nm lasing intensity exhibits a rapid decrease when the control pulse starts overlapping with the pump pulse at around $\Delta t_{\mathrm{pump-control}} = 0$ ps, and then, keeps the lowered intensity, which is kept to be almost constant when the control pulse is in the time range between the pump and seed pulses. It can also be seen in Fig. 3 that, as the energy of the control pulse increases, the lasing signal intensity is reduced to a large extent. This suppression may originate from the promotion of the ionization of N_2, which increases the population in the $X\ ^2\Sigma_g{}^+$ state of $N_2{}^+$ more rapidly than the population transfer from the $X\ ^2\Sigma_g{}^+$ state to the $A\ ^2\Pi_u$ state through postionization coupling [23], as will be discussed in the Theory section below. When the control pulse is injected after the seed pulse, the suppression effect becomes weaker and finally disappears, so that the intensity becomes almost equivalent to that at the negative delay. The time constant (1–3 ps) of this recovery process is consistent with the pulse width of the 391.4-nm lasing at ∼20 mbar [20].

It is also noted in Fig. 3 that a fine modulation can be seen when the control pulse starts overlapping with the seed pulse. This modulation can be ascribed to the fact that the seed pulse experiences a transient refractive index change induced by the control pulse through the impulsive molecular alignment [38], resulting in the seed intensity change which leads to the modulation in the lasing intensity.

Next, we examine the suppression effect of the control pulse on the intensity of the lasing at 391.4 nm integrated over the spectral range of 391.2–391.5 nm in the collinear pump-control scheme [see Fig. 1(b)]. In this measurement, the temporal separation between the pump pulse and the seed pulse is fixed at 5 ps. The polarization directions of the three pulses are all parallel to each other. As shown in Fig. 4, when the energy of the control laser pulse is increased to 400 μJ, the intensity of the 391.4-nm lasing is suppressed in a similar

manner as the suppression of the 391.4-nm lasing shown in Fig. 3. On the other hand, when the energy of the control laser pulse is lowered to 100 μJ, a significant enhancement of the 391.4-nm lasing is identified at the timing of the temporal overlap between the control pulse and the seed pulse. This enhancement becomes pronounced when the control pulse energy is in the range of 50–100 μJ.

It is worth noting that this type of enhancement was not observed in the collinear control-seed scheme. It is possible that the difference in the collinear control-seed scheme shown in Fig. 3 and the collinear pump-control scheme shown in Fig. 4 inherently comes from the cross-measurement method adopted in this study, which leads to the differences in the spatial overlaps of the three laser beams at the interaction region. In addition, the revival structure appearing in the pump-seed delay time range between 0 and 5 ps is less pronounced in Fig. 4 than in Fig. 3. This is because the coaxial seed pulse in the control-seed scheme (Fig. 3) can probe all the molecules driven by the control pulse, while the slightly off-axis seed pulse in the pump-control scheme (Fig. 4) can probe only a part of the molecules driven by the control pulse.

IV. THEORY

In order to understand theoretically the mechanism of the population inversion between the $B\,^2\Sigma_u^+$ ($v = 0$) and $X\,^2\Sigma_g^+$ ($v' = 0$) states of N_2^+ achieved in the 400-nm laser field as well as the mechanism of the suppression of the N_2^+ lasing at 391.4 nm when the 800-nm control laser field is applied, we carried out a numerical simulation by a model including both the postionization coupling of among the $X\,^2\Sigma_g^+$, $A\,^2\Pi_u$, and $B\,^2\Sigma_u^+$ states of N_2^+ [21–23] and the continuous ionizations of N_2 [39–41]. We consider the following equation for the time evolution of the density matrix $\boldsymbol{\rho}$ of the vibronic state of N_2^+:

$$\frac{d\boldsymbol{\rho}(t)}{dt} = -\frac{i}{\hbar}[\boldsymbol{H}(t), \boldsymbol{\rho}(t)] + \boldsymbol{\Gamma}(t), \tag{1}$$

where $[\cdot, \cdot]$ denotes the commutator and $\boldsymbol{\rho}$ denotes the density matrix whose matrix elements $\rho_{\alpha v,\alpha' v'}$ are specified by the electronic state α ($= X$, A, and B) and the vibrational quantum number v. We include vibrational states up to $v_{\max} = 4$ in the simulation. The population $p_{\alpha v}$ in the vibrational state v in the electronic state α is defined by the diagonal matrix element as $p_{\alpha v} = \rho_{\alpha v,\alpha v}$. The Hamiltonian matrix $\boldsymbol{H}$ has the energies $\epsilon_{\alpha v}$ of the vibronic states as diagonal elements, $H_{\alpha v,\alpha v} = \epsilon_{\alpha v}$, and the time-dependent off-diagonal elements read $H_{X v,B v'}(t) = -F(t)\cos\theta\,\mu_{X v,B v'}$ and $H_{X v,A v'}(t) = -F(t)\sin\theta\,\mu_{X v,A v'}$, where $F(t)$ is the laser field, θ is the alignment angle between the molecular axis and the laser polarization vector, and $\mu_{\alpha v,\alpha' v'}$ is the transition dipole moment. The alignment angle θ is assumed to be fixed during the simulation.

The laser field is a sum of the pump laser field and the control laser field and is expressed using the pump-control delay $\Delta t_{\text{pump-control}}$ as $F(t) = f_{\text{pump}}(t) + f_{\text{control}}(t - \Delta t_{\text{pump-control}})$, where $f_x(t) = E_x \cos(\omega_x t + \beta_x t^2)\exp[-(2\ln 2)t^2/\tau_x^2]$, E_x is the peak electric field, ω_x is the angular frequency, β_x is the chirp parameter, τ_x is the pulse width (intensity full width at half maximum), and x stands for either "pump" or "control." The energies $\epsilon_{\alpha v}$ are calculated from the experimentally determined Morse parameters [42], and the numerical values of $\mu_{\alpha v,\alpha' v'}$ are obtained based on the data presented in Refs. [43,44]. The matrix $\boldsymbol{\Gamma}$ is a diagonal matrix in which the diagonal matrix element $\Gamma_{\alpha v,\alpha v}$ is the strong-field ionization rate of N_2 to N_2^+ in the electronic state α and the vibrational state v, calculated by the length gauge strong-field approximation theory [45]. We solve Eq. (1) from $t_i = -1200$ fs to $t_f = 3700$ fs, so that the laser field vanishes before and after the simulation, $F(t_i) = F(t_f) = 0$. The initial condition is $\boldsymbol{\rho}(t_f) = 0$. As shown in Refs. [39–41], Eq. (1) describes simultaneously the time-dependent population dynamics of the vibronic states of N_2^+, the increase in the population by the ionization from N_2, and that by the postionization excitation and deexcitation.

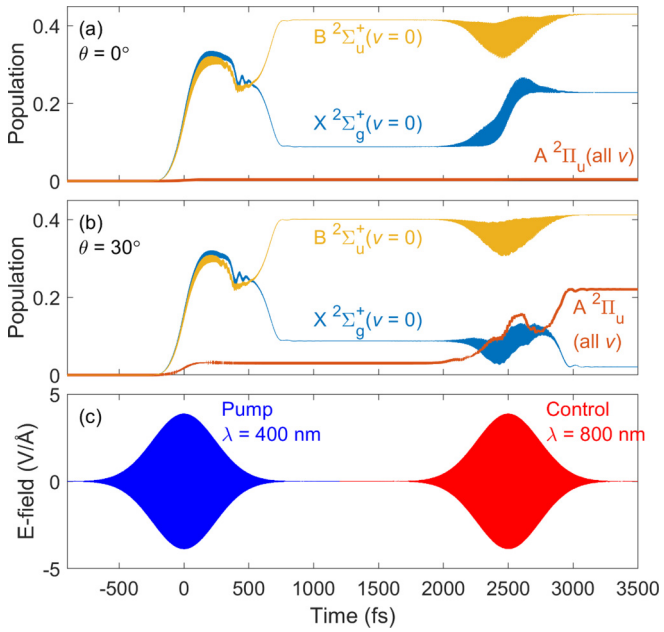

FIG. 5. Time-dependent populations in the $X\,^2\Sigma_g^+(v' = 0)$, $A\,^2\Pi_u$ (summed over v), and $B\,^2\Sigma_u^+(v = 0)$ states for alignment angle (a) $\theta = 0°$ and (b) $\theta = 30°$. The laser field employed in the simulation is shown in (c). Peak field intensity is $I_{\text{pump}} = I_{\text{control}} = 2 \times 10^{14}$ W/cm^2.

The time-dependent populations $p_{X0}(t)$, $p_{B0}(t)$, and $\sum_v p_{Av}(t)$ obtained at the laser parameters $I_{\text{pump}} = I_{\text{control}} = 2 \times 10^{14}$ W/cm^2, $\lambda_{\text{pump}} = 400$ nm, $\tau_{\text{pump}} = \tau_{\text{control}} = 400$ fs, $\beta_{\text{pump}} = \beta_{\text{control}} = 1.03$ fs^{-2}, $\lambda_{\text{control}} = 800$ nm, and $\Delta t_{\text{pump-control}} = 2.5$ ps are shown in Fig. 5 at two alignment angles, that is, $\theta = 0°$, for which the postionization coupling between the $X\,^2\Sigma_g^+$ state and the $A\,^2\Pi_u$ state vanishes [Fig. 5(a)], and $\theta = 30°$ [Fig. 5(b)]. The populations are normalized so that the sum of the final populations becomes equal to 1, that is, $\sum_{\alpha=X,A,B}\sum_{v=0}^{v_{\max}} p_{\alpha v}(t_f) = 1$. We can see that, for both alignment angles, population inversion between the $B\,^2\Sigma_u^+(v = 0)$ state and the $X\,^2\Sigma_g^+$ ($v' = 0$) state is induced by the pump pulse, which is consistent with the experimental observation of the amplification of the seed pulse without the control pulse shown in Fig. 1(d). It should also be noted that the chirped 400-fs pump pulse promotes more the population inversion between $B\,^2\Sigma_u^+$

($v = 0$) and $X\ ^2\Sigma_g^+$ ($v' = 0$) of N_2^+ than a transform-limited pulse at the same laser field intensity, which has been confirmed by our numerical simulations. The interaction with the control pulse leads to an increase in the population of the $X\ ^2\Sigma_g^+$ ($v' = 0$) state in the case of $\theta = 0^\circ$ as can be seen in Fig. 5(a). This increase in the population in the $X\ ^2\Sigma_g^+$ ($v' = 0$) state is ascribed to the additional ionization $N_2^+[X\ ^2\Sigma_g^+(v' = 0)] \leftarrow N_2$ induced by the intense 800-nm control pulse. The increase in the population in the $X\ ^2\Sigma_g^+$ ($v' = 0$) state is a possible mechanism for the suppression of the 391.4-nm lasing intensity for $0 \leqslant \Delta t_{\text{pump-seed}} \leqslant 5$ ps as shown in Figs. 3 and 4. On the other hand, in the case of $\theta = 30^\circ$, because the $X\ ^2\Sigma_g^+$ state and the $A\ ^2\Pi_u$ state are coupled almost resonantly by the 800-nm control pulse, the population in the $A\ ^2\Pi_u$ state increases and the population in the $X\ ^2\Sigma_g^+$ ($v' = 0$) state decreases.

In the model described by Eq. (1), the ionization of N_2 is continuously induced by both the pump and control laser pulses, which is different from the sudden turn-on model adopted in our previous publications [21,23,24], in which we considered that the ionization occurs at the peak of the laser pulse. In the case of a 400-nm pump pulse considered here, the sudden turn-on mechanism in which the frequency bandwidth of the pump pulse experienced by N_2^+ is effectively broadened by the sudden ionization is not crucial for the creation of the population inversion between the $B\ ^2\Sigma_u^+$ state and the $X\ ^2\Sigma_g^+$ state, because the frequency of the pump pulse is already close to resonant with the $B\ ^2\Sigma_u^+ - X\ ^2\Sigma_g^+$ (0, 0) transition.

The results of the simulations have shown that, depending on the alignment angle determining the strength of the postionization $A\ ^2\Pi_u - X\ ^2\Sigma_g^+$ coupling, the control pulse induces either a decrease or an increase of the population in the $X\ ^2\Sigma_g^+$ ($v' = 0$) state, indicating that both an increase and a decrease of the lasing signals become possible and that the extent of molecular alignment is a key factor in controlling the population inversion. The experimental observation of an overall decrease in the 391.4-nm lasing signals achieved when the control pulse is delayed by 0–5 ps with respect to the pump pulse (see Figs. 3 and 4) suggests that the ionization-induced increase in the population in the $X\ ^2\Sigma_g^+$ ($v' = 0$) state in Fig. 5(a) plays a dominant role, because the N-N axis of N_2 is expected to be aligned along the direction parallel to the polarization direction of the control laser pulse by its front part, and ionized subsequently at the timing of the most intense part of the control pulse. Because the transition dipole moment of the $A\ ^2\Pi_u - X\ ^2\Sigma_g^+$ transition is perpendicular to the molecular axis, the postionization $A\ ^2\Pi_u - X\ ^2\Sigma_g^+$ coupling vanishes for molecules aligned along the polarization axis of the control pulse, which means that the population in the $X\ ^2\Sigma_g^+$ state does not decrease by the transition to the $A\ ^2\Pi_u$ state. Therefore, the increase in the population in the $X\ ^2\Sigma_g^+$ state induced by the ionization of the control pulse can lead to a suppression of the lasing signal observed when the timing of the control pulse is set between the pump and seed pulses. When the field intensity of the control pulse becomes lower, it is expected that the population in the $X\ ^2\Sigma_g^+$ state of N_2^+ created by the tunnel ionization of N_2 becomes lower, resulting in the enhancement of the extent of the population inversion between the $B\ ^2\Sigma_u^+$ and $X\ ^2\Sigma_g^+$ state by the efficient depletion of the population in the $X\ ^2\Sigma_g^+$ state through the $A\ ^2\Pi_u - X\ ^2\Sigma_g^+$ resonance pumping by the control laser pulse. Consequently, the enhancement of the $B\ ^2\Sigma_u^+ - X\ ^2\Sigma_g^+$ lasing intensity is achieved at the weaker energy of the control laser pulse shown in Fig. 4. We finally remark that, even though we have shown above that the experimentally observed suppression of the lasing signal can be explained by assuming that N_2^+ is aligned along the polarization direction of the control pulse, a more quantitative comparison of the theoretically calculated population inversion and the experimentally observed lasing signal would require a dynamical treatment of the rotational motion of N_2^+, including both the impulsive alignment during the pump and control laser pulses and the field-free rotation in the time zone between the control and pump pulses.

V. SUMMARY

In summary, we have experimentally demonstrated the forward lasing emission of N_2^+ at 391.4 nm induced by the 400-nm laser field and found that the inverted populations mainly result from the rotational levels of $J' = 7$–17 in the excited $B\ ^2\Sigma_u^+(v = 0)$ state of N_2^+. We have further shown that the intensity of the lasing emission can be modulated by applying an additional control 800-nm pulse between the pump and the seed pulses. By including the continuous ionization of N_2 and the multistate coupling among the $B\ ^2\Sigma_u^+$, $A\ ^2\Pi_u$, and $X\ ^2\Sigma_g^+$ states in N_2^+ in the theoretical model, we have revealed that the population inversion in N_2^+ can be achieved by the 400-nm pump laser and further modulated by the control pulse, in which the possible increase and decrease of the population in the $X\ ^2\Sigma_g^+$ ($v' = 0$) state of N_2^+ by the dynamic competition between the ionization of N_2 and the population transfer from $X\ ^2\Sigma_g^+$ ($v' = 0$) to $A\ ^2\Pi_u$ in N_2^+ induced by the control pulse plays a critical role in the suppression of the N_2^+ lasing. Our results clarify the role of the ionization of N_2 by an independent control pulse in the N_2^+ lasing, which provides a different route to the manipulation and control of the N_2^+ lasing induced by an intense laser field.

ACKNOWLEDGMENTS

The work is supported by National Natural Science Foundation of China (Grants No. 62027822 and No. 11904121), and JSPS KAKENHI (Grants No. JP15H05696, No. JP20H00371, and No. JP21K04990).

[1] T. Popmintchev, M. C. Chen, D. Popmintchev, P. Arpin, S. Brown, S. Ališauskas, G. Andriukaitis, T. Balčiunas, O. D. Mücke, A. Pugzlys, A. Baltuška, B. Shim, S. E. Schrauth, A. Gaeta, C. Hernández-García, L. Plaja, A. Becker, A. Jaron-Becker, M. M. Murnane, and H. C. Kapteyn, Bright coherent ultrahigh harmonics in the keV X-ray regime from mid-infrared femtosecond lasers, Science **336**, 1287 (2012).

[2] J. Posthumus, The dynamics of small molecules in intense laser fields, Rep. Prog. Phys. **67**, 623 (2004).

[3] G. Mourou, Nobel Lecture: Extreme light physics and application, Rev. Mod. Phys. **91**, 030501 (2019).

[4] D. Strickland, Nobel Lecture: Generating high-intensity ultrashort optical pulses, Rev. Mod. Phys. **91**, 030502 (2019).

[5] H. Zang, H. Li, W. Zhang, Y. Fu, S. Chen, H. Xu, and R. Li, Robust and ultralow-energy-threshold ignition of a lean mixture by an ultrashort-pulsed laser in the filamentation regime, Light Sci. Appl. **10**, 49 (2021).

[6] T. Liang, H. Zang, W. Zhang, L. Zheng, D. Yao, H. Li, H. Xu, and R. Li, Reliable laser ablation ignition of combustible gas mixtures by femtosecond filamentating laser, Fuel **311**, 122525 (2022).

[7] Q. Luo, W. Liu, and S. L. Chin, Lasing action in air induced by ultra-fast laser filamentation, Appl. Phys. B **76**, 337 (2003).

[8] A. Dogariu, J. B. Michael, M. O. Scully, and R. B. Miles, High-gain backward lasing in air, Science **331**, 442 (2011).

[9] J. Yao, B. Zeng, H. Xu, G. Li, W. Chu, J. Ni, H. Zhang, S. L. Chin, Y. Cheng, and Z. Xu, High-brightness switchable multiwavelength remote laser in air, Phys. Rev. A **84**, 051802(R) (2011).

[10] H. Xu, Y. Cheng, S. L. Chin, and H. Sun, Femtosecond laser ionization and fragmentation of molecules for environmental sensing, Laser Photon. Rev. **9**, 275 (2015).

[11] H. Li, H. Zang, Y. Su, Y. Fu, and H. Xu, Generation of air lasing at extended distances by coaxial dual-color femtosecond laser pulses, J. Opt. **19**, 124006 (2017).

[12] X. Zhao, S. Nolte, and R. Ackermann, Lasing of N_2^+ induced by filamentation in air as a probe for femtosecond coherent anti-Stokes Raman scattering, Opt. Lett. **45**, 3661 (2020).

[13] H. Li, E. Lötstedt, H. Li, Y. Zhou, N. Dong, L. Deng, P. Lu, T. Ando, A. Iwasaki, Y. Fu, S. Wang, J. Wu, K. Yamanouchi, and H. Xu, Giant Enhancement of Air Lasing by Complete Population Inversion in N_2^+, Phys. Rev. Lett. **125**, 053201 (2020).

[14] M. Britton, M. Lytova, D. H. Ko, A. Alqasem, P. Peng, D. M. Villeneuve, C. Zhang, L. Arissian, and P. B. Corkum, Control of N_2^+ air lasing, Phys. Rev. A **102**, 053110 (2020).

[15] N. Dong, Y. Zhou, S. Pang, X. Huang, K. Liu, L. Deng, and H. Xu, Strong-field-induced N_2^+ air lasing in nitrogen glow discharge plasma, Chin. Phys. Lett. **38**, 043301 (2021).

[16] Y. Fu, S. Chen, S. Wang, W. Zhang, D. Yao, H. Zang, H. Li, and H. Xu, Asymmetric enhancement of N_2^+ lasing in intense, birefringence-modulating elliptical laser fields, Opt. Express **28**, 23274 (2020).

[17] Y. Fu, J. Cao, S. Wang, S. Chen, H. Zang, H. Li, E. Lötstedt, T. Ando, A. Iwasaki, K. Yamanouchi, and H. Xu, Extremely enhanced N_2^+ lasing in filamentary plasma grating in ambient air, Opt. Lett. **46**, 3404 (2021).

[18] H. Li, D. Yao, S. Wang, Y. Fu, and H. Xu, Air lasing: Phenomena and mechanisms, Chin. Phys. B **28**, 114204 (2019).

[19] X. M. Tong, Z. X. Zhao, and C. D. Lin, Theory of molecular tunneling ionization, Phys. Rev. A **66**, 033402 (2002).

[20] Y. Liu, P. Ding, G. Lambert, A. Houard, V. Tikhonchuk, and A. Mysyrowicz, Recollision-induced Superradiance of Ionized Nitrogen Molecules, Phys. Rev. Lett. **115**, 133203 (2015).

[21] H. Xu, E. Lötstedt, A. Iwasaki, and K. Yamanouchi, Sub-10-fs population inversion in N_2^+ in air lasing through multiple state coupling, Nat. Commun. **6**, 8347 (2015).

[22] J. Yao, S. Jiang, W. Chu, B. Zeng, C. Wu, R. Lu, Z. Li, H. Xie, G. Li, C. Yu, Z. Wang, H. Jiang, Q. Gong, and Y. Cheng, Population Redistribution among Multiple Electronic States of Molecular Nitrogen Ions in Strong Laser Fields, Phys. Rev. Lett. **116**, 143007 (2016).

[23] T. Ando, E. Lötstedt, A. Iwasaki, H. Li, Y. Fu, S. Wang, H. Xu, and K. Yamanouchi, Rotational, Vibrational, and Electronic Modulations in N_2^+ Lasing at 391 Nm: Evidence of Coherent $B^2\Sigma_u^+ - X^2\Sigma_g^+ - A^2\prod_u$ Coupling, Phys. Rev. Lett. **123**, 203201 (2019).

[24] H. Li, M. Hou, H. Zang, Y. Fu, E. Lötstedt, T. Ando, A. Iwasaki, K. Yamanouchi, and H. Xu, Significant Enhancement of N_2^+ Lasing by Polarization-Modulated Ultrashort Laser Pulses, Phys. Rev. Lett. **122**, 013202 (2019).

[25] Y. Fu, E. Lötstedt, H. Li, S. Wang, D. Yao, T. Ando, A. Iwasaki, F. H. M. Faisal, K. Yamanouchi, and H. Xu, Optimization of N_2^+ lasing through population depletion in the $X^2\Sigma_g^+$ state using elliptically modulated ultrashort intense laser fields, Phys. Rev. Res. **2**, 012007(R) (2020).

[26] A. Mysyrowicz, R. Danylo, A. Houard, V. Tikhonchuk, X. Zhang, Z. Fan, Q. Liang, S. Zhuang, L. Yuan, and Y. Liu, Lasing without population inversion in N_2^+, APL Photonics **4**, 110807 (2019).

[27] M. Richter, M. Lytova, F. Morales, S. Haessler, O. Smirnova, M. Spanner, and M. Ivanov, Rotational quantum beat lasing without inversion, Optica **7**, 586 (2020).

[28] R. Danylo, G. Lambert, Y. Liu, V. Tikhonchuk, A. Houard, and A. Mysyrowicz, Quantum erasing of laser emission in N_2^+, Opt. Lett. **45**, 4670 (2020).

[29] Z. Liu, J. Yao, J. Chen, B. Xu, W. Chu, and Y. Cheng, Near-resonant Raman Amplification in the Rotational Quantum Wave Packets of Nitrogen Molecular Ions Generated by Strong Field Ionization, Phys. Rev. Lett. **120**, 083205 (2018).

[30] S. Wang, E. Lötstedt, J. Cao, Y. Fu, H. Zang, H. Li, T. Ando, A. Iwasaki, K. Yamanouchi, and H. Xu, Population inversion in N_2^+ by vibrationally mediated Rabi oscillation at 400 nm, Phys. Rev. A **104**, 032823 (2021).

[31] T. J. Wang, J. F. Daigle, J. Ju, S. Yuan, R. Li, and S. L. Chin, Forward lasing action at multiple wavelengths seeded by white light from a femtosecond laser filament in air, Phys. Rev. A **88**, 053429 (2013).

[32] A. Zhang, M. Lei, J. Gao, C. Wu, Q. Gong, and H. Jiang, Subfemtosecond-resolved modulation of superfluorescence from ionized nitrogen molecules by 800-nm femtosecond laser pulses, Opt. Express **27**, 14922 (2019).

[33] S. Wang, Y. Fu, D. Yao, S. Chen, W. Zhang, H. Li, and H. Xu, Observation of the optical $X^2\Sigma_g^+ - A^2\prod_u$ coupling in N_2^+ lasing induced by intense laser field, Chin. Phys. B **28**, 123301 (2019).

[34] M. Britton, M. Lytova, P. Laferriere, P. Peng, F. Morales, D. H. Ko, M. Richter, P. Polynkin, D. M. Villeneuve, C. Zhang, M. Ivanov, M. Spanner, L. Arissian, and P. B. Corkum, Short- and long-term gain dynamics in N_2^+ air lasing, Phys. Rev. A **100**, 013406 (2019).

[35] H. Zhang, C. Jing, J. Yao, G. Li, B. Zeng, W. Chu, J. Ni, H. Xie, H. Xu, S. L. Chin, K. Yamanouchi, Y. Cheng, and Z. Xu, Rotational Coherence Encoded in an "Air-Laser" Spectrum of Nitrogen Molecular Ions in an Intense Laser Field, Phys. Rev. X **3**, 041009 (2013).

[36] R. R. Laher and F. R. Gilmore, Improved fits for the vibrational and rotational constants of many states of nitrogen and oxygen, J. Phys. Chem. Ref. Data **20**, 685 (1991).

[37] Y. Zhang, E. Lötstedt, T. Ando, A. Iwasaki, H. Xu, and K. Yamanouchi, Rotational population transfer through the $A^2\prod_u - X^2\Sigma_g{}^+ - B^2\Sigma_u{}^+$ coupling in $N_2{}^+$ lasing, Phys. Rev. A **104**, 023107 (2021).

[38] C. Marceau, S. Ramakrishna, S. Genier, T. Wang, Y. Chen, F. Theberge, M. Chateauneuf, T. Seideman, and S. L. Chin, Femtosecond filament induced birefringence in argon and in air: Ultrafast refractive index change, Opt. Commun. **283**, 2732 (2010).

[39] Q. Zhang, H. Xie, G. Li, X. Wang, H. Lei, J. Zhao, Z. Chen, J. Yao, Y. Cheng, and Z. Zhao, Sub-cycle coherent control of ionic dynamics via transient ionization injection, Commun. Phys. **3**, 50 (2020).

[40] Z. Li, Y.-H. Kuan, X. Mu, Z. Miao, C. Wu, and W.-T. Liao, Ramsey interferometry through coherent $A^2\prod_u - X^2\Sigma_g{}^+ - B^2\Sigma_u{}^+$ coupling and population transfer in $N_2{}^+$ air laser, Opt. Lett. **45**, 6587 (2020).

[41] V. T. Tikhonchuk, Y. Liu, R. Danylo, A. Houard, and A. Mysyrowicz, Modeling of the processes of ionization and excitation of nitrogen molecules by short and intense laser pulses, Phys. Rev. A **104**, 063116 (2021).

[42] K. P. Huber, G. H. Herzberg, J. W. Gallagher, and R. D. Johnson, III, Constants of diatomic molecules, in *NIST Chemistry Web-Book, NIST Standard Reference Database Number 69*, edited by P. J. Linstrom and W. G. Mallard (National Institute of Standards and Technology, Gaithersburg, MD, 2021).

[43] S. R. Langhoff, C. W. Bauschlicher, and H. Partridge, Theoretical study of the $N_2{}^+$ Meinel system, J. Chem. Phys. **87**, 4716 (1987).

[44] S. R. Langhoff and C. W. Bauschlicher, Jr., Theoretical study of the first and second negative systems of $N_2{}^+$, J. Chem. Phys. **88**, 329 (1988).

[45] T. K. Kjeldsen and L. B. Madsen, Strong-field ionization of N_2: Length and velocity gauge strong-field approximation and tunnelling theory, J. Phys. B: At. Mol. Opt. Phys. **37**, 2033 (2004).